PZT Sensor Array for Local and Distributed Measurements of Localized Cracking in Concrete

Article *in* Smart Materials and Structures · June 2018

DOI: 10.1088/1361-665X/aaca4d

3 authors:

Arun Narayanan
Indian Institute of Technology Hyderabad
10 PUBLICATIONS **27** CITATIONS

Amarteja Kocherla
Indian Institute of Technology Hyderabad
5 PUBLICATIONS **4** CITATIONS

Kolluru Subramaniam
Indian Institute of Technology Hyderabad
130 PUBLICATIONS **1,481** CITATIONS

PZT Sensor Array for Local and Distributed Measurements of Localized Cracking in Concrete

PZT Sensor Array for Local and Distributed Measurements of Localized Cracking in Concrete

Arun Narayanan[a], Amarteja Kocherla[a] and Kolluru V. L. Subramaniam[a1]

[a] Department of Civil Engineering, Indian Institute of Technology Hyderabad, Hyderabad, TS 502285, INDIA

Abstract

An application is developed with surface mounted Lead Zirconate Titanate (PZT) patches for sensing damage in the form of a stress-induced crack in a concrete substrate. A localized crack is introduced in a controlled manner using a fracture test. Full-field displacements obtained using digital image correlation are used for crack penetration and crack width measurements. Electrical impedance (EI) measurements are obtained from the individual PZT patches, which are attached at different locations relative to the crack. Stress wave transmission measurements are performed using the PZT patches as actuator-receiver (AR) pairs. The EI measurements indicate that small, quantifiable changes in the mechanical impedance of the substrate are experienced by the PZT patch in the vicinity of the localized crack, which sensitively detect crack initiation. The stress wave-based measurements are very sensitive to the presence of physical discontinuity created by a localized crack in the stress wave path. A measure of stress wave attenuation, the attenuation factor is developed, to quantify the measured changes in the stress wave produced by the physical discontinuity in concrete upon

[1] Corresponding Author: Professor, Department of Civil Engineering, Indian Institute of Technology Hyderabad, Hyderabad, TS 502205, INDIA. ph.:+91-402-301-6093, email: kvls@iith.ac.in

unloading a stress-induced crack. The physical discontinuity due to a stress-induced crack opening on the order of 10μm can be detected from the measured changes in the attenuation factor. The physical discontinuity in the concrete associated with a stress-induced crack opening on the order of 100 μm produces a complete attenuation of the stress wave of 120 kHz. The combined use of PZT patches in the EI and the AR modes can be used to detect local changes close to a PZT patch and it allows distributed sensing over the entire volume of a structural element.

1. Introduction

PZT is a piezoelectric material, which is being used for developing economical methods for continuous damage assessment in structures. PZT exhibits a coupled electromechanical (EM) response; surface charges are produced when mechanical strain is induced and strain when electrical potential is applied. PZT-based sensors offer a significant potential for continuously monitoring the development and progression of internal damage in structures. Several damage detection strategies have been developed using PZT patches attached to a substrate [Song et al. (2008), Zhu and He (2011), Lim et al (2012), Lu et al. (2013), Rucka and Wilde (2013), Divsholi and Yang (2014), Narayanan and Subramaniam (2016a, b), Liang et al. (2016), Huo et al. (2017), Ai et al. (2017)]. The use of PZT patches has been primarily focused on metallic and composite structures with very limited application to concrete. The use of PZT patches in concrete structures is still evolving.

The electrical impedance (EI) obtained from the measured electrical response of a PZT patch at multiple frequencies depends on the electromechanical (EM) response of the PZT material, the geometry of the patch and the boundary conditions. The electrical impedance measurements from a PZT patch bonded to a substrate depend on the EM response of the coupled system. When a PZT patch is attached to a substrate, the dynamic motion of the PZT patch in response to an applied electrical potential depends on the dynamic mechanical impedance to its motion provided by the substrate, the mechanical impedance [Liang et al. (1994), Giurgiutiu et al. (1999), S. Park et al. (2006), Na and Lee (2012), Narayanan et al. (2017)]. The use of a PZT patch to infer about the level of damage in the substrate requires interpreting the coupled EM response of the PZT patch attached to the substrate. Understanding the response of PZT patch attached to a concrete substrate is still evolving. Changes are registered in EI measurements due to formation of cracks well in advance of failure [Park et al. (2000)]. The EM impedance (EMI) derived from the electrical measurements on PZT patches attached to a concrete substrate sensitively detect changes in the local material compliance produced by distributed damage in the vicinity of the sensor [Narayanan and Subramaniam (2016a, b)]. For a PZT patch attached to a concrete substrate, its motion at a given frequency is directly influenced by a zone of influence, which represents the finite volume of material. The EMI measurements from a concrete substrate are shown to be sensitive to incipient distributed damage in the material within the zone of influence [Narayanan et al. (2018)]. A smaller zone of influence and higher sensitivity to local changes increases at higher frequencies. The EI measurements therefore provide a local measure of damage in the vicinity of the sensor.

The coupled constitutive electro-mechanical response of piezoelectric material allows a PZT patch to be used as an actuator for generating stress waves in the substrate material and as a receiver for sensing stress waves. The PZT patches are used as actuator/receiver (AR) pairs for generating and receiving stress waves. In the distributed sensing mode, damage in the material is inferred through changes in the elastic waves which propagate through the bulk material [Jung et al. (2002), Aggelis and Shiotani (2007), Marani et al. (2014)]. Presence of cracks in the wave propagation has been shown to significantly alter the wave characteristics

[Lu et al. (2013), Watanabe et al. (2014), Kee and Nam (2015), Luo et al. (2016)]. Most of the studies of PZT-based distributed monitoring were reported on metallic structures. The condition monitoring of concrete infill in fiber reinforced polymer tubes and failure in concrete and composite structures has been monitored using PZT sensor arrays [Xu et al. (2017), Memmolo et al. (2016), Divsholi and Yang (2014), Lu et al. (2013)]. Most of the researchers used time of flight and decrease in wave energy to assess changes in the material characteristics.

In concrete, damage initiation takes place in the form of distributed micro cracks, which eventually coalesce to form localized cracks. Cracks in concrete are associated with cohesive crack bridging stresses. There may be significant degradation of the capacity of the structure by the time of appearance of visible cracking on the surface of a concrete structure. Initiation of early intervention measures, which can effectively increase the service life of the structure require early detection of damage. Methods to detect incipient damage in the form of micro cracks are required to provide effective methods of monitoring structural health and service life performance of structures. Procedures for locating cracks in concrete and for assessing the depth of opening of these cracks is critical for evaluating the degradation of concrete structures.

Localized sensing methodology based on EI technique provides information about changes in the local material, which produce changes in its compliance in the vicinity of PZT patch. Any damage located away from the sensing range of a PZT patch would not be detected in its EM signature. In concrete structures where large volume of material has to be monitored a large number of PZTs is required for local sensing. Sensing methodology using pairs of PZT patches for monitoring changes in the stress wave can be used for distributed sensing over a larger region. Local sensing technique (EI measurements) can be employed to detect the damage in the vicinity of the PZT patches while distributed sensing using PZT sensor arrays can be used to monitor the location and the magnitude of damage in a region. The concept of array of sensors which combines both local and distributed sensing using minimum number of sensors provides detailed interpretation about the damage.

A sensing scheme using an array of PZT sensors for combined local and distributed damage monitoring is developed. Surface mounted PZT patches are used for continuous local monitoring of concrete and obtaining the information related to damage in the vicinity of the patch. Additionally, the PZT sensor array is used for monitoring damage in the actuator-receiver (AR) mode. The results of an experimental evaluation involving the use of a fracture test specimen are presented and issues related to the development of proposed system are evaluated for the case of localized damage in the form of a crack in concrete. The sensitivity of the EM impedance-based local measurements and the through-transmission measurements to a localized crack in concrete is evaluated.

2. Background

PZT patches are made of piezoceramic materials, which have high electro-mechanical coupling properties. The electrical impedance (inverse of admittance) signature of the PZT patch can be measured when it is excited with an alternating electrical potential. The electrical impedance is a complex number consisting of real and imaginary parts, and is determined as the ratio of the current to the applied voltage. The electrical conductance response (real part of electrical admittance) of a PZT patch (20 mm x 20 mm x 1 mm size) when an alternating potential excitation of 1 V amplitude over a range of frequencies between 10 kHz and 500 kHz, is shown in **Figure 1**. The peaks in the conductance response can be identified with the resonant modes of the PZT patch [Liang et al. (1994), Xu and Liu (2002]. The mechanical and the electromechanical resonances happen at the same frequency in a piezoelectric material because of the electro-mechanical coupling. The electro-mechanical resonance frequencies of the PZT patch depends on the mechanical resonances which in turn depends on geometry of the patch [Giurgiutiu (2001)].

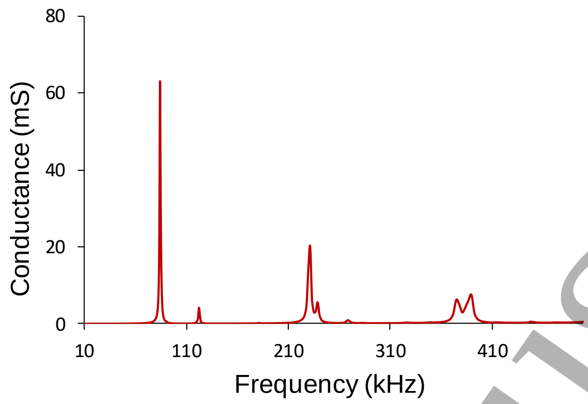

Figure 1. Electrical conductance spectrum of a free PZT patch (patch size: 20 mm x 20 mm x 1 mm)

The EI response of a PZT patch attached to the substrate subjected to an applied electrical potential depends on the dynamic impedance to its motion from the substrate. The resistance to the motion of a PZT patch from the surrounding elastic medium is expressed as the mechanical impedance. Most approaches for modeling the PZT patch-structure interaction have varied in the degree of sophistication in representing the motion of the PZT patch and the structure. The first systematic attempt to model the PZT patch-structure interaction was presented by Liang et al. (1994) using a PZT actuator driven one-degree-of-freedom spring-mass-damper system. Subsequently, for a PZT patch, an effective 1-D approach was found to give a better representation of the dynamic response of the PZT considering in-plain motion of the PZT coupled to an elastic substrate [Bhalla and Soh (2004)]. The frequency dependent complex admittance response of the PZT patch, $\bar{Y}$ is given as

$$\bar{Y} = \frac{4\omega i l^2}{h}\left[\overline{\varepsilon_{33}^T} - \frac{2d_{31}^2\overline{Y^E}}{(1-\nu)} + \frac{2d_{31}^2\overline{Y^E}Z_{a,eff}}{(1-\nu)(Z_{s,eff}+Z_{a,eff})}\left(\frac{\tan\kappa l}{\kappa l}\right)\right] \tag{1}$$

where $Z_{a,eff}$ and $Z_{s,eff}$ are the mechanical impedances of the PZT and the substrate, respectively; l and h are the half-length and the thickness of the PZT patch, respectively; ν is the Poisson's ratio of the piezoelectric material; $\overline{\varepsilon_{33}^T}$ is complex dielectric constant; $\overline{\varepsilon_{33}^T} = \varepsilon_{33}^T\,(1-\delta i)$; δ=dielectric loss factor; $\overline{Y^E}$ is the complex modulus of PZT given as $\overline{Y^E} = Y^E(1+i\eta)$; η is the mechanical loss factor; d_{31} is the piezoelectric strain constant; k is the wave number which is calculated as $k = \omega\sqrt{\frac{\rho(1-\nu^2)}{\overline{Y^E}}}$; ρ is the density of the PZT material; E is the electric field applied for actuation with circular frequency ω and i is $\sqrt{-1}$.

A change in the mechanical impedance of the surrounding medium changes the EI response of the PZT patch. For a concrete substrate, the effective dynamic response of the PZT patch was shown to be influenced by the damping and the stress in the substrate [Narayanan and Subramaniam (2016b)]. Considering the high material damping of concrete, the dynamic response of a PZT patch attached to a concrete substrate exhibits a frequency dependence. The vibratory motion of the PZT patch is influenced by the mechanical impedance derived from a zone of finite size. For a PZT patch attached to the concrete substrate, the dynamic response, which consists of distinct modes of vibration of the PZT patch is significantly influenced by the compliance of the material within a zone of influence. The zone of influence for the vibratory motion of a bonded PZT patch depends on the frequency of vibration; the zone of influence is smaller for higher frequencies [Park et al. (2000), Zagrai and Giurgiutiu (2001), Narayanan et al. (2018)]. Any changes in the material compliance within the zone of influence, influences the vibratory motion of the PZT patch. Distributed damage produces an increase in the compliance and the level of damping of the material. Both these effects are known to produce a downward shift in frequency and decrease in amplitude of the resonant mode in the EI spectrum.

In this study, an array of surface mounted PZT patches are used for combined EI and AR measurements. As shown in **Figure 2**, an array of PZT patch sensors is deployed in a structural element, where the EI measurement from the PZT patch is used for local monitoring while the through-transmission measurements are used for distributed sensing. Each PZT patch is used as an actuator and a sensor for through-transmission measurements in the AR mode. A schematic representation of the methodology is given in **Figure 2**. A received signal undergoes the losses due to signal propagation path and in epoxy at the concrete-beam interfaces. Measures for quantifying changes in the EMI and the received waves due to damage in the form of a localized crack are developed for the level of material discontinuity produced by a stress-induced crack of a given opening.

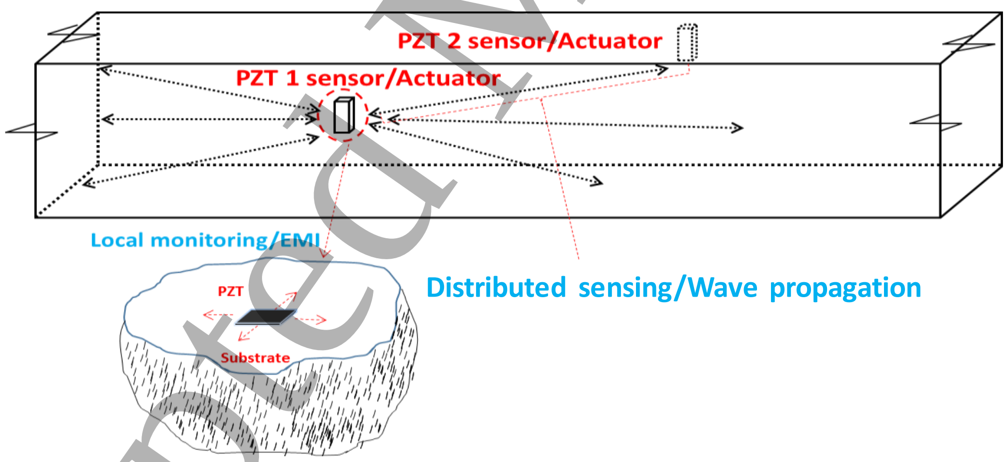

Figure 2. Schematic representation of local-distributed monitoring system using surface mounted PZT patches.

3. Materials and Methods

The details of the concrete used in this study is given in **Table 1**. Coarse aggregate consisted of 20 mm and 10 mm crushed gravel in a 1:1 proportion and river sand was used as fine aggregate. Cement conforming to the requirements of OPC grade 53 as per the Indian code of practice, IS 12269:2013 was used. The 28-day compressive strength and modulus of rupture obtained by testing standard 150 mm cubes and 500 mm x 150 mm x 150 mm sized beams. The properties of the concrete are given in **Table 1**.

The experimental program consisted of using PZT patches in the distributed (AR) mode and for local EI-based measurements on beams where the damage is induced in the form of a localized crack. A fracture beam was used to produce a crack under flexural loading. The experiments were conducted using notched concrete beams of size 500 mm (length) x 150 mm (height) x 150 mm (width), made with plain cement concrete. A notch, 25 mm in depth was introduced in the middle and fracture tests were performed using a computer-controlled, servo–hydraulic testing machine The test setup consisted of third point loading as per the requirements of UNI 11039-2:2003 standard. The flexure test was conducted with a span equal to 450 mm in four-point bending configuration. The fracture test was conducted in crack mouth opening displacement (CMOD) control. The CMOD was increased at rate of 30 μm/minute. During the test, the crack tip opening displacement (CTOD) was also measured using a clip gauge mounted at the tip of the notch. Six square 20 mm PZT patches of 1 mm thickness were attached to each beam. Properties of the PZT is given in **Table 2**. Two PZT patches were bonded on front face and two on back face, remaining two were attached to the soffit of the beam. The PZT patches labelled PZT5 and PZT6 were positioned at the bottom of the beam, 50 mm away from the notch. The other PZT patches were bonded at mid-height of the beam. The PZT patches labelled PZT2 and PZT4 were attached on opposite faces and were located at a distance of 50 mm from the center of the beam. The PZT patches labelled PZT1 and PZT3 were attached on opposite faces of the beam at a distance 50 mm away from the end of the beam. All the PZT patches were bonded to concrete using a two component epoxy. The properties of the epoxy are given in **Table 3**. The complete test set up showing the locations of the gauges and the PZT sensors is shown in **Figure 3a**.

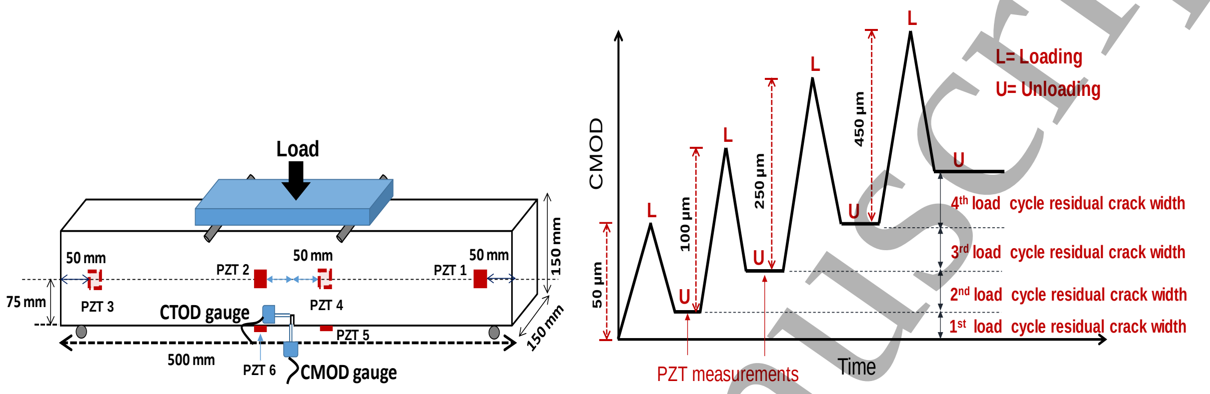

(a) (b)

Figure 3. (a) Test set up for fracture tests with configuration of PZT patches (b) Cyclic loading showing the progressive increase in CMOD.

The test program consisted of cyclic, incremental loading to a larger crack opening in every subsequent cycle; the beam was progressively loaded to predefined values of CMOD. The loading program is shown schematically in **Figure 3b**. Initially, the beam was loaded up to a CMOD equal to 50 µm and unloaded. In the subsequent load cycle, the specimen was loaded to a CMOD value equal to 100 µm relative to the CMOD in the unloaded configuration. In subsequent load cycles, the CMOD was increased to values equal to 250 µm and 450 µm with respect to the residual crack openings at the end of second and third cycles, respectively. In the text, the first, the second, the third and the fourth load cycles are referred to by the maximum relative CMOD values equal to 50 µm, 100 µm, 250 µm and 450 µm, respectively.

Table 1. Properties of the concrete

Mix proportion (cement: water: fine aggregate: coarse aggregate)	Density (kg/m^3)	Compressive strength (MPa)	Young's modulus (GPa)	Modulus of Rupture (MPa)
1:0.45: 1.85: 2.89	2320	50	33	3.6

Table 2. Properties of the PZT material

Properties	Values
Elasticity matrix	$C_E = \begin{bmatrix} 1.20 \times 10^{11} & 7.51 \times 10^{10} & 7.50 \times 10^{10} & 0 & 0 & 0 \\ 7.51 \times 10^{10} & 1.20 \times 10^{11} & 7.50 \times 10^{10} & 0 & 0 & 0 \\ 7.50 \times 10^{10} & 7.50 \times 10^{10} & 1.10 \times 10^{11} & 0 & 0 & 0 \\ 0 & 0 & 0 & 2.10 \times 10^{10} & 0 & 0 \\ 0 & 0 & 0 & 0 & 2.10 \times 10^{10} & 0 \\ 0 & 0 & 0 & 0 & 0 & 2.25 \times 10^{10} \end{bmatrix} Pa$
Piezoelectric Constants	$d = \begin{bmatrix} 0 & 0 & 0 & 0 & 5.84 \times 10^{-10} & 0 \\ 0 & 0 & 0 & 5.84 \times 10^{-10} & 0 & 0 \\ -1.71 \times 10^{-10} & -1.71 \times 10^{-10} & 3.74 \times 10^{-10} & 0 & 0 & 0 \end{bmatrix} C/N$
Relative permittivity	$e = \begin{bmatrix} 1730 & 0 & 0 \\ 0 & 1730 & 0 \\ 0 & 0 & 1700 \end{bmatrix}$

Poisson's ratio, v	Density, ρ (kg/m^3)	Dielectric loss factor, δ	Damping ratio, ζ	Mechanical quality factor, Q_m
0.35	7700	0.02	0.006	75

Table 3. Properties of the Epoxy

Young's modulus (GPa)	Poisson's ratio	Density (kg/m^3)
2	0.36	1300

The EI measurements were performed on all the PZTs before attaching to the beam. The EI measurements were performed at an applied voltage of 1 V over 800 discrete frequencies ranging between 10 kHz and 500 kHz. A 6500B series impedance analyzer of Wayne Kerr make was used for the electrical measurements. The measurements from the PZT patches after attaching to the concrete beam consisted of EI measurements from the individual PZT patches and through transmission measurements from pairs of PZT patches in the AR mode. A schematic sketch of the test setup used for measurements from the PZT patches is shown in **Figure 4.** The impedance and the wave propagation measurements were taken after unloading from the predetermined value of CMOD. The experimental set up for the EI and the AR measurements consisted of an impedance analyzer, a function generator, an amplifier, a digital storage oscilloscope and a computer. In the AR mode, the waveform generated by the function generator was amplified and sent to the actuator PZT. Then, the response signal of the remaining five PZTs were logged by the computer, which was interfaced with the digital storage oscilloscope. After acquiring the wave propagation data from all the PZTs, the actuator PZT was switched to the impedance analyzer through the switching unit and the EI measurements were recorded. A typical conductance (real part of admittance) signature of the a PZT patch bonded to beam is shown in **Figure 4**. This measurement procedure was followed when the specimen is in unloaded state after each load cycle (unloading from CMOD openings equal to 50 μm, 100 μm, 250 μm and 450 μm, relative to the previous unloaded configuration).

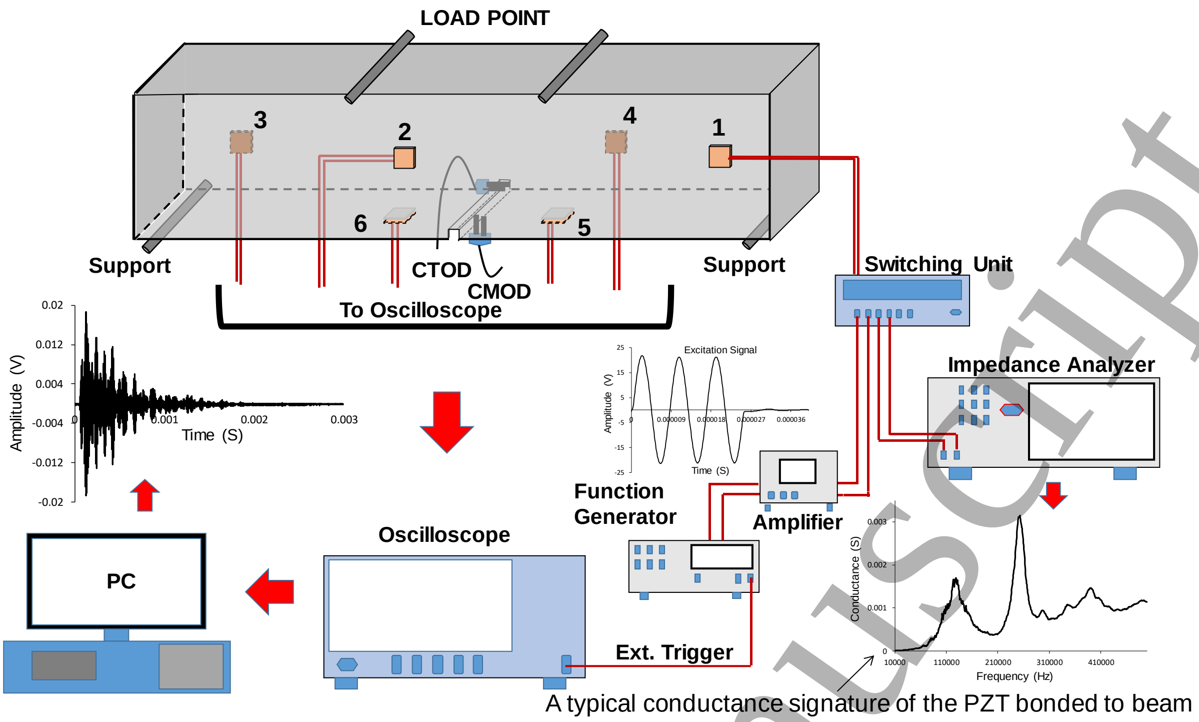

Figure 4. Experimental setups for EI measurements from individual PZT patches and through transmission measurements from pairs of PZT patches in the AR mode.

In the AR mode, the excitation applied to the PZT patches consisted of a 3-cycle tone burst sine signal with center frequency of 120 kHz with a 45 V peak-to-peak voltage at a pulse repeating frequency equal to 100 Hz (**Figure 5a**). The center frequency of 120 kHz was selected to match with the center frequency of the first resonance peak of the bonded PZT to provide higher input and higher sensitivity to received wave. The first resonance peak of the bonded PZT occurs at a low frequency and has the highest energy when compared to other resonance frequencies, which results in lower attenuation of the transmitted waves and a larger received signal. A typical received signal at PZT2 when PZT 1 was actuated (A_1R_2) is shown in **Figure 5b**. All the six PZT patches were individually excited and the response from the all other PZT patches were collected at a sampling frequency of 6.25 MHz.

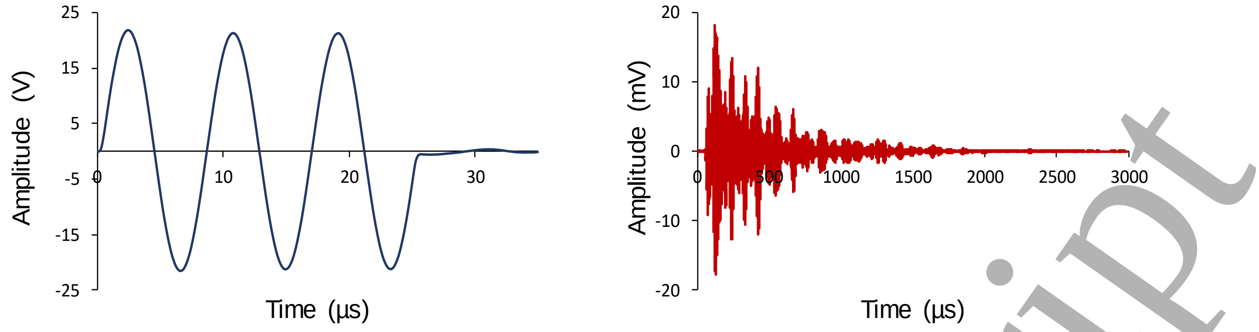

(a) (b)

Figure 5. Signals from a through-transmission measurement in the AR mode: (a) The excitation signal applied to the actuator (b) The received signal at PZT2 when actuating PZT1 (A_1R_2)

During the loading cycles, full-field surface displacements from the beam were obtained using digital image correlation (DIC). DIC measurements were performed on notched specimens to monitor the localization of damage and the subsequent propagation of a crack. DIC relies on correlation between images of specimens in the deformed and the reference unstressed state. A spray painted speckle pattern was created on the surface of the beam. The front face of the beam was initially painted white to create a uniform background. A random pattern was created with a mist of black paint, which was sprayed on the white background. After seating the specimen in the loading setup, the front face of the specimen was uniformly lit with white light. During the flexure test, digital images of the specimen were captured using a camera which was fitted with a 50 mm lens and was placed at a distance of 1 m from the specimen surface. A schematic representation of the DIC setup is shown in **Figure 6**. A digital image of the specimen, referred to as the reference image was captured prior to initiation of loading. Images of the specimen were captured during the loading program. Each image was 5 mega pixels and physical calibration was established to be in the range of 12-14 pixels per mm.

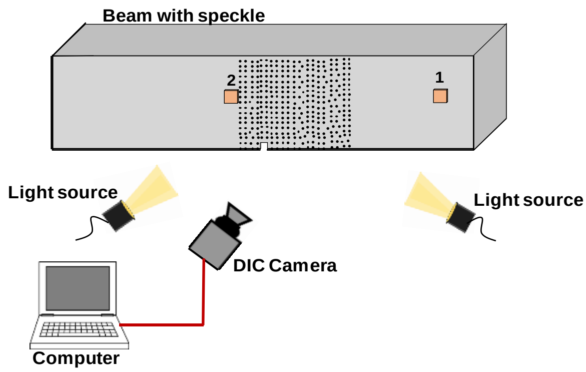

Figure 6. Schematic representation of the DIC setup.

Spatially continuous surface displacements are obtained from correlation between of the random speckle pattern in the deformed and the reference images of the specimen. Analysis for correlations and pattern identification was performed within small neighborhoods called subsets [Bruck et al. (1989), Schreier and Sutton (2002)]. Within each subset, a unique pattern of grey level distribution is formed because of the random sprayed-on pattern. The grey-level pattern in each subset differs from other subsets. The correspondence between matching subsets in images of the specimen in the reference and the deformed states was established using spatial domain cross-correlation. The mapping of positions within the reference image to positions in the deformed images was performed using second-order, two-dimensional shape functions. Sub-pixel level accuracy was obtained using the Quintic B-spline interpolation of the gray values. The cross correlation analysis of the digital images was performed using the VIC-2D^{TM} software. Strains were calculated from the displacement gradients at each loading stage, by evaluating the shape functions and their partial derivatives at the center of the subset. In the analysis, a subset of size 29 pixels x 29 pixels was used. For the setup used in this study, the random error in the measured displacement was in the range of 0.002 pixels and the resolution accuracy of strain was determined to be 1 μm.

4. Experimental Results

The load-CMOD responses of three beam specimens are shown in **Figure 7a** and the load-CMOD response of one beam is shown in **Figure 7b** for clarity. The beam was tested in four stages. In each stage, the beam was loaded in CMOD control to a predetermined crack opening relative to the beginning of load cycle and then unloaded to zero load. The EI and wave propagation measurements were taken in the unloaded configuration. The quasi-static load response can be readily identified with the load envelope obtained from the load cycles. The peak load of the envelope load response is attained in the first load cycle. CMOD equal to 50 μm is in the post-peak part of the softening load response. There is a continuous increase in the residual CMOD on unloading after each loading cycle. There is also correspondingly a decrease in the stiffness of the load-CMOD response. With every subsequent load cycle, the peak load attained is also smaller.

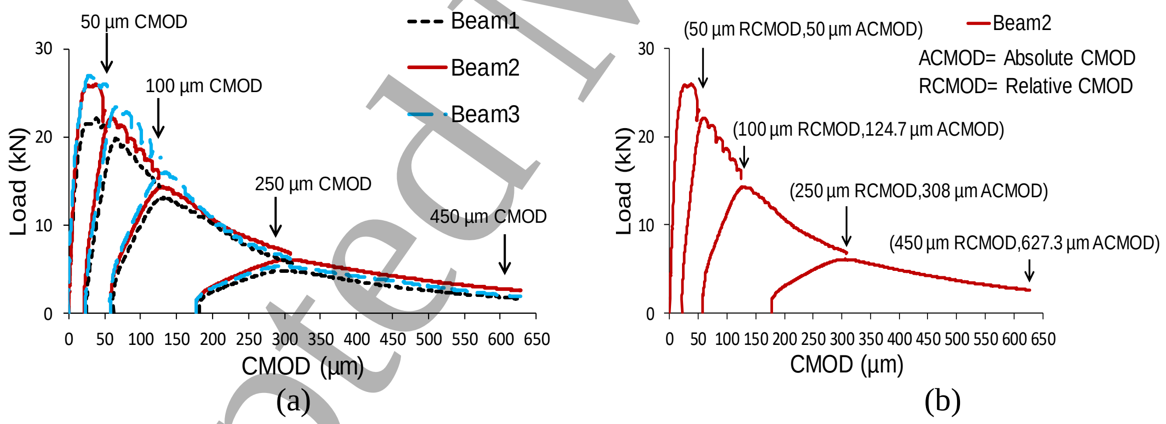

Figure 7. (a) Load-CMOD responses of beams; (b) Load-CMOD of Specimen Beam 2. The CMOD relative to the residual CMOD for each cycle are shown. The absolute value of CMOD at the end of each cycle is also indicated in the bracket.

Contours of horizontal strain (ε_{xx}) from the beam specimen 2 at different CMOD values obtained using DIC are plotted in **Figure 8**. The contours of strain are plotted at the top of the load cycle, just prior to unloading. Localization of the strain can be identified in all the contour plots. The location of the crack can be clearly identified even at a small CMOD equal to 50 μm. The localized zone propagates along the depth of the beam with increasing CMOD. While the crack could be identified in the contours of ε_{xx} even at a small CMOD of 50 μm, the crack could not be delineated visually up to a CMOD of 124 μm. There is a sharp gradient in strain within a small region centered on the crack. In the region in the immediate vicinity of the PZT patch, the magnitude of strain is very small and there is no visible damage which produces variation in the measured strain. There is also no visible damage in the form of micro cracking in the region away from the crack.

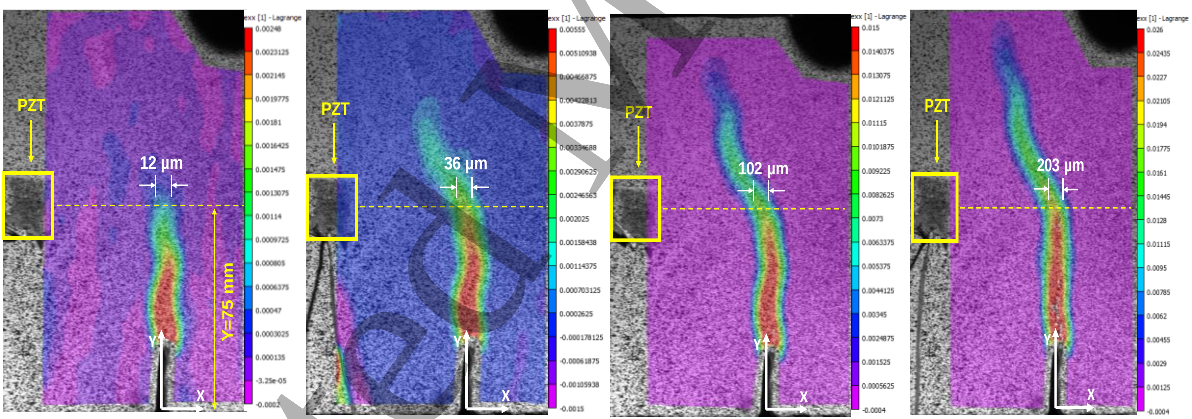

(a) (b) (c) (d)

Figure 8. Strain contour ($\boldsymbol{\varepsilon_{xx}}$) at different CMOD levels (a) 50 μm (b) 100 μm relative to unloading after first load cycle (up to an absolute CMOD equal to 124.7 μm) (d) 250 μm relative to unloading after second load cycle (up to an absolute CMOD equal to 308 μm) (e) 450 μm relative to unloading after third load cycle (up to an absolute CMOD equal to 627 μm)

The horizontal strain (ε_{xx}) along length of the beam at the mid-height location along a line with Y coordinate fixed at 75 mm above the bottom face and 50 mm above the notch for various CMOD levels are shown in **Figure 9**. The variation of ε_{xx} along the length shows a sharp increase in the magnitude of strain indicating localization of strain within a small region centered on the notch. It is observed that the width of the localization remains relatively constant with increasing crack opening. With increasing crack opening at the soffit of the beam given by the CMOD, there is an increase in the magnitude of maximum strain. There is also correspondingly a sharper strain gradient within the region of localization with increasing CMOD.

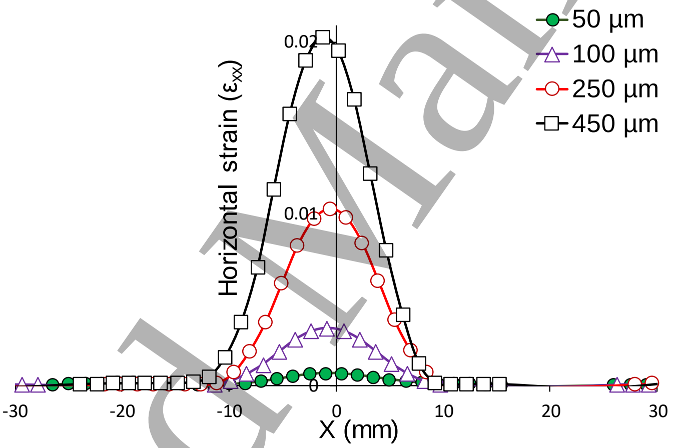

Figure 9. Variation in the horizontal strain (ε_{xx}) with X coordinate for a line located at Y = 75 mm from the bottom of the beam at different values of relative CMOD after each unloading.

The 3D contours of horizontal displacement (U_x) obtained at the end of the last load cycle when the CMOD was increased to 450 µm from the unloaded configuration, is shown in **Figure 10a**. The crack in the medium is identified by the displacement discontinuity emanating from the notch. The profile of the crack is identified by the sudden increase in the U_x over a

363 small region. The discontinuity in U_x introduced by the crack emanating from the notch is evident in the jump in the U_x. The presence of the crack and the associated physical opening within a subset resulted in a loss of correlation within the subsets in which the crack was present. The loss of correlation and the finite size of the pixel resulted in smearing of the displacement gradient within a region of size equal to the subset size close to the crack. The actual width of the region of localization produced by the crack is therefore smaller than the width of the zone with high strains indicated in **Figure 9**. A procedure for obtaining the crack opening precisely, free from the error introduced by the finite subset size was developed using the asymptote matching procedure [Reddy and Subramaniam (2017), Gali and Subramaniam (2018)]. The crack opening widths along the depth of the beam at different values of CMOD obtained using the asymptote matching procedure and are shown in **Figure 10b** for beam specimen 2. The CMOD corresponds to the displacement measured across the notch at Y=0, using the CMOD gauge located at the bottom of the beam. The CMOD is also shown marked in the figure at the location corresponding to Y=0. The crack opening widths were determined from the U_x measured using DIC. Corresponding to the CMOD measured on the soffit of the beam, there is a decrease in the crack opening width with increasing Y coordinate above the notch. The zero crack opening along the depth of the beam gives the physical location of the tip of the propagating crack. The observed crack opening as a function of depth for different values of CMOD indicates that the crack tip progresses along the depth of the beam with increasing CMOD. For a CMOD of 50μm, the crack has propagated along the depth and the tip of the crack can be identified at 86 mm from bottom of the beam and the corresponding crack opening at the mid-height location is 12 μm. At a CMOD equal to 100 μm relative to unloaded configuration at the end of the first load cycle (absolute CMOD equal to 124.7 μm), the tip of the crack is located at Y= 119 mm and the crack opening at the mid-height location is 36 μm. In the subsequent load cycles when the CMOD is increased to 250 μm and 450μm

relative to the unloaded CMOD from the previous cycles, the crack advances to a depth of 124 mm and 135 mm, respectively. The corresponding crack openings at the mid-height are 102 µm and 203 µm, respectively.

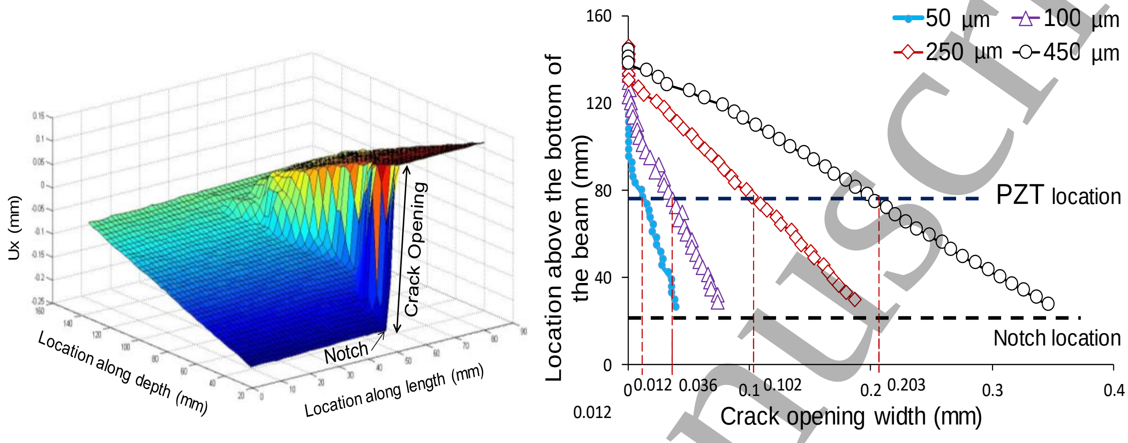

(a) (b)

Figure 10. (a) Contour showing crack opening displacement at the relative value of CMOD = 450µm after the third cycle; (b) Crack opening width as a function of depth of the beam at different crack mouth opening displacements.

4.1 Measurements from PZT patches

The stress wave attenuation measurements were performed in the unloaded state, where the removal of the load results in closing of the crack. The measured changes recorded by the PZT patches therefore correspond to the physical discontinuity in the medium produced by the stress-induced crack. Each PZT patch was individually actuated (**Figure 11b**) and the responses were recorded at all the other PZT patches. This measurement procedure was repeated when the specimen was in the unloaded state after pre-determined crack opening indicated by different relative values of CMOD (50 µm, 100 µm, 250 µm and 450 µm). The level of noise obtained from the standard deviation of the initial part of the signal was on the order of 0.1 mV. All the received signals were conditioned with a linear phase, band-pass filter. A comparison of actual received signal and filtered received signal is shown in **Figure 11a**. **Figure 11b** shows a typical signal received by PZT2 using PZT1 as the actuator (A_1R_2) at the seating load, prior to initiation of the first cycle of loading. The received signal is significantly smaller in magnitude when compared with the excitation. The decrease in the magnitude of the received signal is attributed to losses in the path of the wave produced by the geometric spreading of the wave and the material attenuation in the wave path in the epoxy and in the concrete. There is also a significant increase in the length of the received wave when compared with the excitation applied, which is due to several effects such as, the ringing of the PZT patch, geometric spreading and multiple reflections, mode conversions and from inhomogeneity of the beam specimen [Aggelis and Shiotani (2007)].

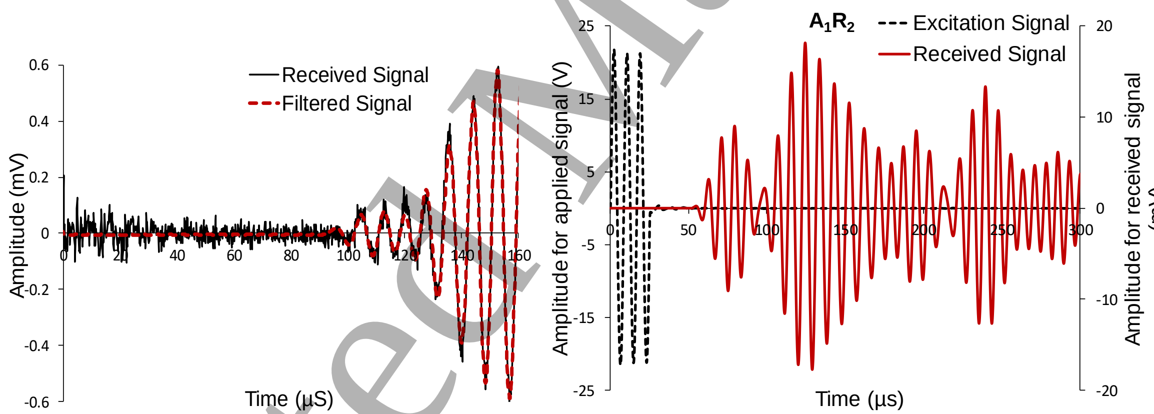

(a) (b)

Figure 11. (a) Comparison of the actual received and the filtered received signal (b) Comparison of the actuating signal with sensor signal prior to loading and the received signal after filtering.

Figure 12 shows the signals recorded from different PZT sensors (PZT2, PZT4, PZT6) when PZT1 was actuated. The received signals at PZT6 have a smaller amplitude when compared with the signals recorded by PZT2 and by PZT4 even in the pristine stage. The amplitude of the signal is influenced by the material and geometric attenuation in path of the transmission. Each subfigure in **Figure 12** shows the variation in the received signal in the unloaded state after each cycle. The changes recorded at the different PZT patches however vary depending on the positions of the PZT patches relative to the notch. With increasing CMOD, there was a decrease in the amplitude and an increase in the time of arrival of the stress waves received at PZT2 and PZT6 when compared with the corresponding baseline signatures. The changes in the received waves are produced by the presence of the crack in the path of stress wave propagation. The received signals of PZT4 are not significantly altered since the wave path does not intersect the crack. The received signals at PZT4 exhibit a small change which may be attributed to stress wave reflection from the crack surface.

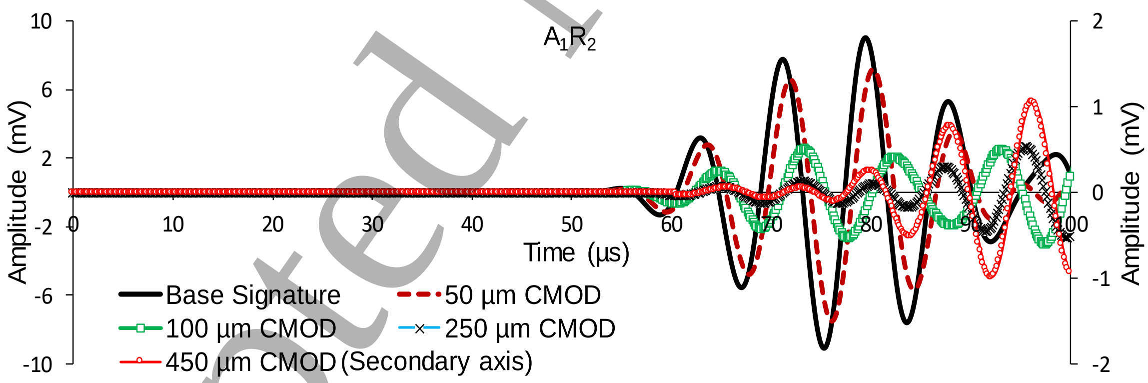

(a)

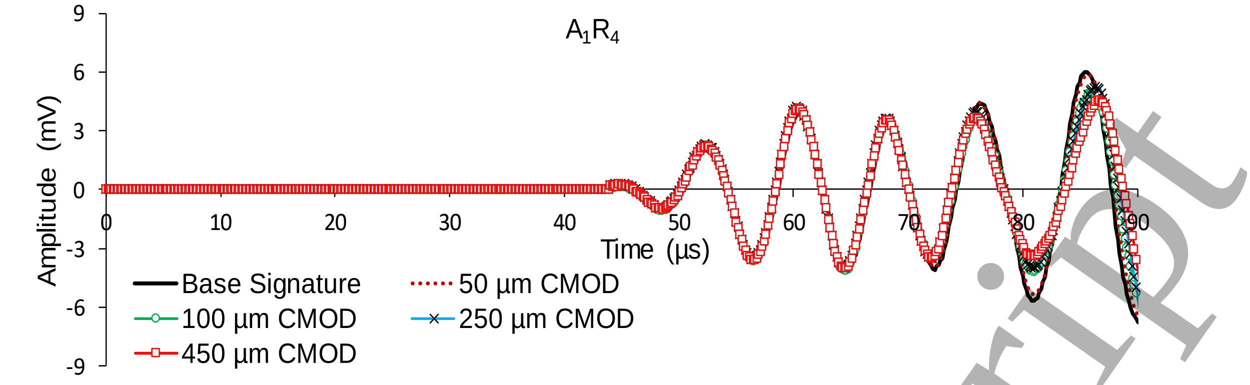

(b)

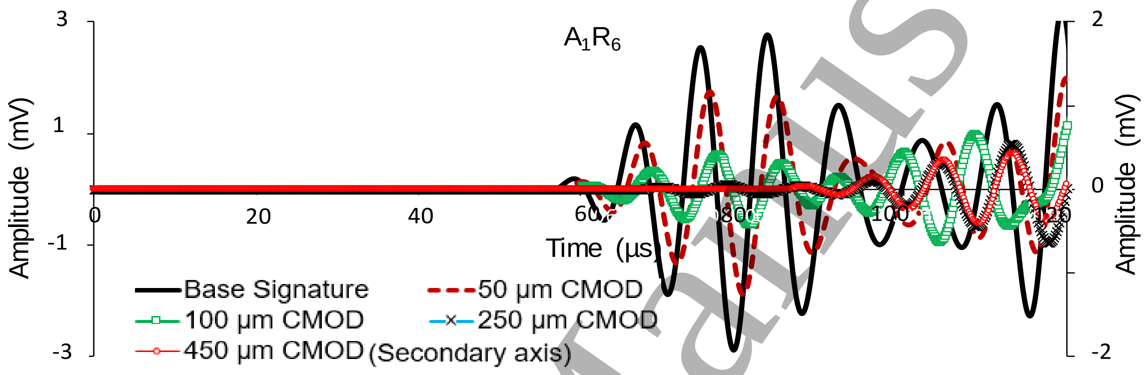

(c)

Figure 12. The received signals when PZT1 is actuated for different crack opening displacements: (a) received at PZT2 (b) received at PZT4 (c) received at PZT6.

When PZT1 is actuated, the stress wave signals received at the other PZT patches depend on the stress wave transmission path. Any changes in the received signal characteristics are produced by changes in the stress wave transmission path. When comparing the sensor signals after each load cycle with base line signature, the signals received at PZT 2 and PZT6 undergo changes in the time of arrival and the energy content. The contours of ε_{xx} shown in **Figure 9** also show that there was ε_{xx} concentration beyond the mid height of the beam in the A_1R_2 transmission path for all four CMOD levels. There is an increasing level of material discontinuity in the propagation path produced by the crack after each load cycle.

Correspondingly, there is a larger decrease in the amplitude and a larger increase in the arrival time in the received signals. After the first load cycle, the crack was not visually apparent and was only detected from the displacement discontinuity recorded using DIC. From the crack opening width as a function of height shown in **Figure 10b**, for a CMOD equal to 50 µm, the crack propagating depth was 86 mm from bottom of the beam and the crack opening displacement at the mid-height in the loaded configuration was 12 µm. The crack propagated beyond the direct wave path of A_1R_2 (actuating PZT1 and receiving PZT2) even at the CMOD equal to 50 µm.

Typical electrical conductance spectra recorded from EI measurements from the six PZT patches attached at different locations on the beam specimen 2 are shown in **Figure 13**. Distinct resonance modes are clearly identified with peaks in the spectra. The relative locations and amplitudes of the peaks in the conductance spectra are relatively constant. The variations in the absolute values of amplitudes and the center frequencies of the individual peaks are due to variations in the properties of the individual PZT patches and the thickness of the epoxy used for bonding the PZT patch to the concrete substrate. The first and the second resonance peaks are centered on 120 kHz and 250 kHz, respectively. The peaks of resonance have previously been shown to be sensitive to changes in substrate compliance within their respective zones of influence [Narayanan and Subramaniam (2016a, b)]. The zones of influence for the first and the second resonant peaks for 1 mm thick, 20 mm square patches have been shown to be 150 mm and 100 mm, respectively. The local peaks on the first resonant peak are identified with the influence of the boundary of the specimen, which is within its zone of influence [Narayanan et al. (2018)]. The presence of distributed damage, which influences the mechanical impedance of the substrate in the zone of influence has been shown to produce changes in the amplitude and center frequency of the resonant peak.

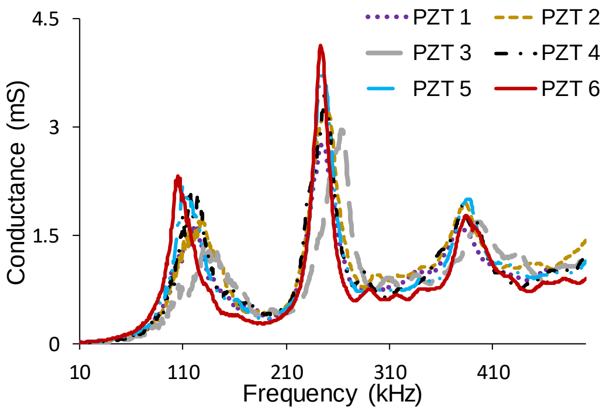

Figure 13. The electrical conductance spectra recorded from the PZT patches

The EI measurements were recorded from the PZT patches in the unloaded state. The conductance spectra over frequencies centered on the first and second peaks for PZT2 and PZT5 (50mm away from notch) and PZT3 (180mm away from notch) are shown in **Figure 14**. The electrical conductance obtained from the PZTs centered on the first resonant peak are shown in **Figures 14 a, b, c.** A change is noticed in the EI response of all the PZTs. As the crack is located away from the zone of influence of first peak for PZT 3, the changes are minimal. For PZT 2 and PZT5, there are irregular changes identified in the local peaks due to the presence of the material discontinuity within the zone of influence of the first peak of the PZTs.

The electrical conductance obtained from the PZTs centered on the second peak are shown in **Figures 14 d, e, f.** There were no changes in the second peak of EM response of PZT 3 since the crack lies outside its zone of influence [Narayanan et al. (2018]. There are small changes in conductance signatures centered on the second resonant peak for PZT2 and PZT5 at the different levels of CMOD as the crack passes through the zones of influence. The measurements from DIC indicated that the crack was very localized while the material away from the localized zone had no damage. Considering no visible distributed damage, the presence of localized damage within the zone of influence does not appear to significantly influence the mechanical impedance offered by the concrete medium to the motion of the PZT in the second resonant mode. The second resonant mode is therefore not sensitive to the presence of a localized material discontinuity produced by a stress-induced crack in concrete.

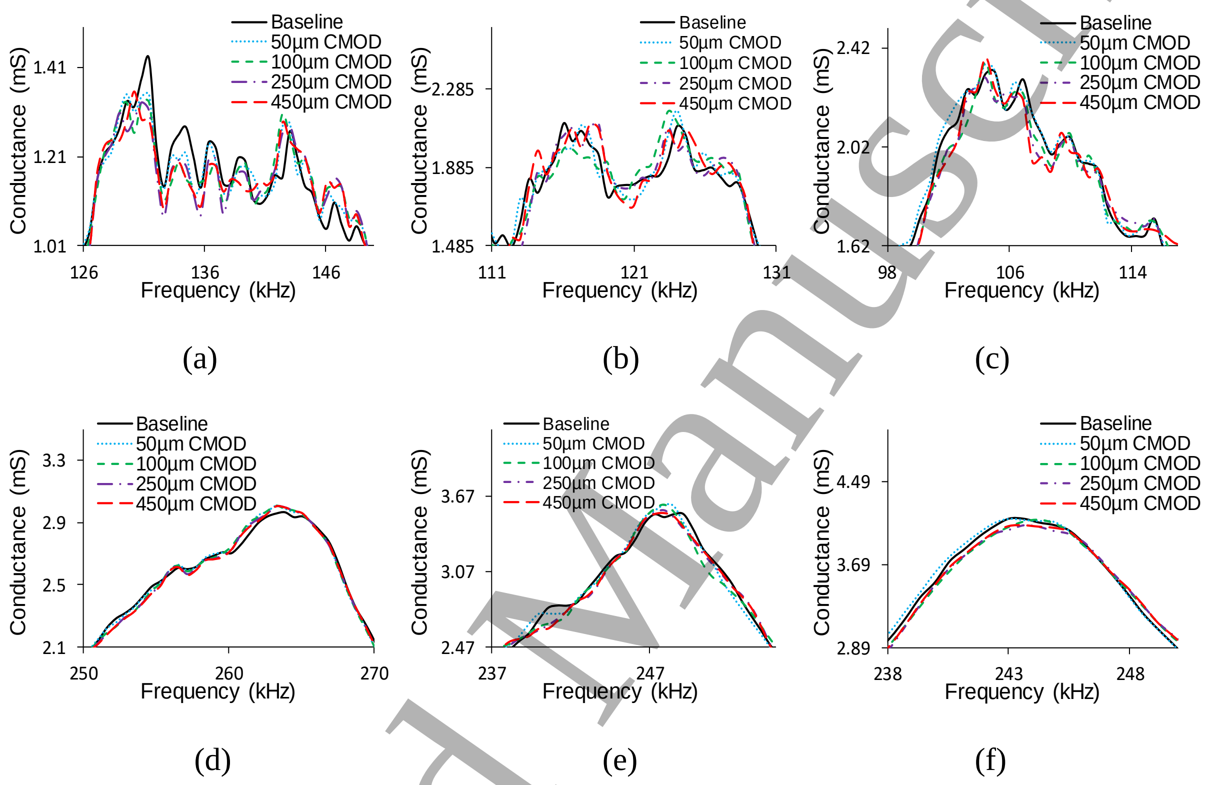

Figure 14. Electrical conductance spectra close to first peak at different CMOD levels of (a) PZT 3 (b) PZT 2 (c) PZT 5. Conductance spectra close to second peak at different CMOD levels of (d) PZT 3 (e) PZT 2 (f) PZT 5.

5. Analysis of Results

The experimental studies conducted on the beam at different levels of CMOD indicate that there is a consistent change in the recorded parameters induced by the localized crack. The stress-induced crack in concrete is associated with a physical opening under applied loading

518 and it produces a discrete discontinuity in the material in the unloaded state. The discrete crack
519 present in the concrete is also very localized and does not produce any additional strain or
520 damage in the bulk of the medium. From the DIC measurements it was established that even
521 at a CMOD equal to 50 μm, the crack had propagated to a depth of 86 mm above the notch.
522 The physical opening at the mid-height was determined to be 12 μm in the loaded state when
523 the CMOD was 50 μm. With an increase in the CMOD there was an increase in the physical
524 crack opening along the depth of the crack. The opening displacement produced by a stress
525 induced crack creates a physical discontinuity in the material medium. The measurements from
526 the PZT patches were performed in the unloaded state, and these correspond to the material
527 discontinuity produced by the stress-induced crack.

528 A quantification of the observed changes is performed to identify the changes in the wave
529 characteristics and the EI measurements produced by the presence of the localized crack in the
530 medium. In the AR measurements, the changes are observed in the time of flight of stress wave
531 arrival and in the amplitude of stress wave. Percentage changes in the time of flight (TOF) and
532 the attenuation factor (A(*f*)) were used to quantify the changes in the received signal in the AR
533 mode. Changes in the conductance signature at the resonance peaks of the EI response were
534 quantified using the root mean square deviation (RMSD).

535 The changes in propagation path of stress wave due to material discontinuity produce changes
536 in the time of flight (TOF) of the received signal. The percentage (%) change in the TOF at
537 each level of CMOD was calculated using Equation (2), where $(TOF)_d$ is the TOF at different
538 CMOD and $(TOF)_0$ is the TOF at zero CMOD. Time of flight of the signals were calculated
539 using voltage thresholding technique where a threshold value (5 μV) was set for the signal and
540 the time at which the received signal crosses threshold is taken as TOF. The threshold voltage
541 was set based on maximum noise level present in the signal.

$$\Delta TOF(\%) = \frac{[(TOF)_d - (TOF)_0]}{(TOF)_0} * 100 \quad (2)$$

The ΔTOF(%) for the different AR pairs are plotted as a function of the different stress-induced crack opening at the mid-height of the beam in **Figure 15**. The physical crack opening at the mid-height location of the beam determined using DIC are used for the plot. The values corresponding to reverse excitation of PZTs are not plotted since these values were nominally identical. After the first cycle of loading, there is an increase in the ΔTOF(%) in the received signals at the different PZTs. In the AR pairs, where the wave path did not intersect the crack, there was no change in the ΔTOF(%). In the subsequent load cycles when the relative value of CMOD was equal to 100 µm, 250 µm and 450 µm there is a further increase in the ΔTOF(%) for in the AR pairs with signal path crossing the crack (A_6R_5, A_1R_3, A_3R_4. A_4R_6, A_3R_5 and A_1R_6). The measurements in ΔTOF% progressively increase with an increase in the physical discontinuity in the concrete produced by the stress-induced crack associated with the measured opening.

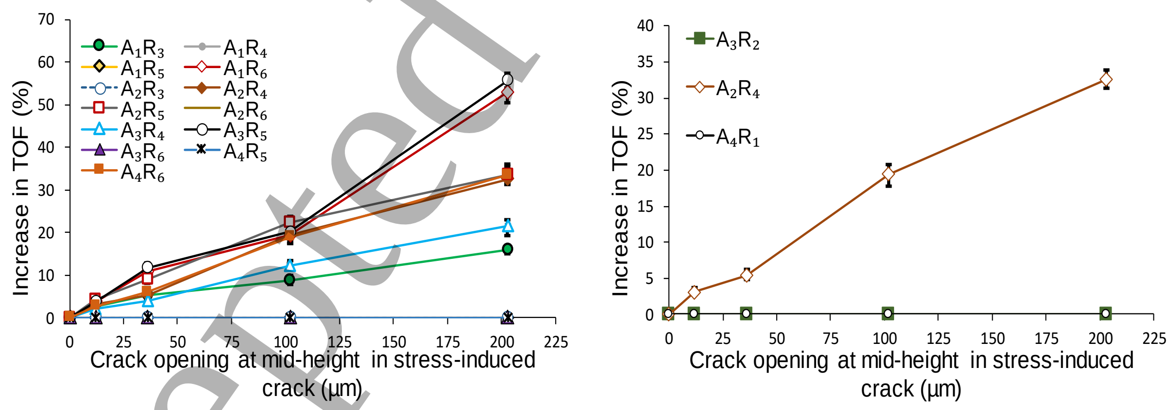

(a) (b)

Figure 15. (a) ΔTOF(%) at different CMOD values. b) ΔTOF(%) for transmission paths A_3R_2, A_2R_4 and A_4R_1

The ΔTOF(%) for transmission paths A_3R_2- A_2R_4- A_4R_1, which connect PZTs located at mid-height, are plotted as a function of stress-induced crack opening in the stress wave path in **Figure 15b**. There is no change on the ΔTOF(%) measured in the signal path A_3R_2, A_4R_1. In the path A_2R_4 there is consistent increase in ΔTOF(%) with an increase in the stress induced crack opening. Changes in the time of flight of the received signal are attributed to the presence of the material discontinuity in the stress wave path. The ΔTOF(%) therefore provides a reliable parameter for detecting changes in the transmission of the stress wave due to the discontinuity in the material medium produced by a localized stress-induced crack in concrete.

A comparison between the actuated signal and the received signal prior to initiation of loading indicates that there is significant attenuation in the path of wave. When one PZT pair is used in the AR mode it is of interest to determine the additional attenuation produced by the material damage. The influence of attenuation in the stress wave path produced by the materials, concrete and epoxy, have to be separated to determine the additional attenuation produced by the crack. The changes in the received signals due to the propagation of crack depend on the distance between actuator and sensor, depth and width of crack. In an array of sensors where comparison among different transmission paths are necessary to identify the location and the severity of the crack, a new damage index known as Attenuation factor ($A(f)$) is introduced in the analysis for compensating the intervening effects such as properties of PZTs, amplitude of the resonance frequencies of PZTs, epoxy concrete interface losses and length of direct propagation path. The procedure is similar to the self-calibrating technique where the signal processing in the AR mode consisted of normalizing signals in the frequency domain [Achenbach et al. (1992), Wang and Subramaniam (2011)]. The received signal in time domain signal was transformed to the frequency domain using the FFT algorithm. The direct stress transmission in an AR pair is the stress wave in the early part of the received signal. The signal received subsequently contains reflections from the boundaries and edges. The initial 26 µs (length of actuating signal) signal starting from time of flight of the received signal was taken as the direct stress wave (non-reflected signal) as shown in the **Figure 16a**. The FFT of non-reflected time domain signal with the corresponding half power bandwidth was shown in **Figure 16b.**

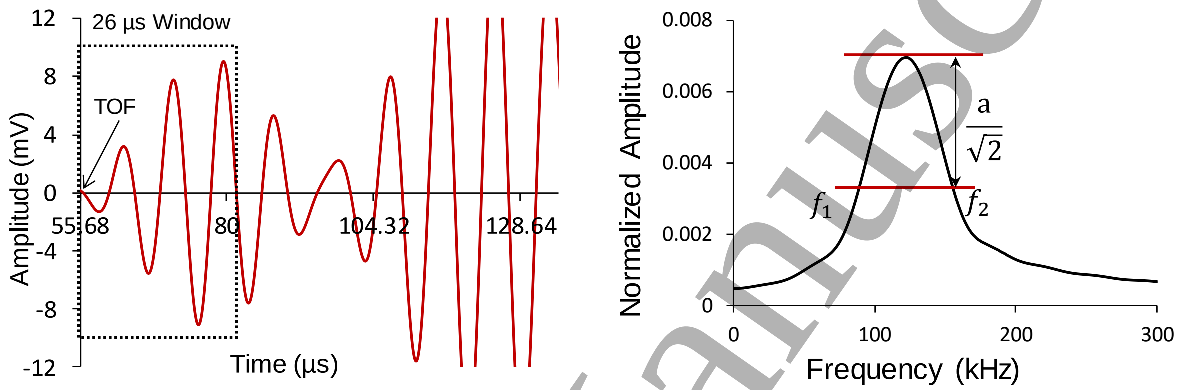

(a) (b)

Figure 16. (a) Non-reflected signal (26 µs) (b) FFT of the received non-reflected time domain signal (26 µs)

The received signal in a through transmission measurement in time domain contains influences of losses due to propagation media and can be expressed as,

$$r_s = a_s * l_{ea} * l_{sp} * l_{es} \quad (3)$$

where r_s is the received signal, a_s is the actuating signal, l_{ea}, l_{es} are the signal losses in the layer of epoxy present at the actuator and sensor, respectively, l_{sp} is the due to propagation through concrete, and '$*$' is the convolution operator. The received signals at zero CMOD $(r_s(f)_0)$ and at different CMOD levels $(r_s(f)_d)$ can be expressed as,

$$r_s(f)_0 = a_s(f).\, l_{ea}(f).\, l_{sp}(f).\, l_{es}(f \tag{4}$$

$$r_s(f)_d = a_s(f).\, l_{ea}(f).\, l_{sp}(f).\, l_{es}(f).\, L_d(f) \tag{5}$$

where $r_s(f)_0, r_s(f)_d$ are the magnitudes of FFT at zero and CMOD equal to d, $L_d(f)$ is signal loss due to crack. $L_d(f)$ is calculated from equation (4) and (5) as,

$$L_d(f) = \left(\frac{r_s(f)_d}{r_s(f)_0}\right) \tag{6}$$

The attenuation factor, $A(f)$ was determined as the average of $L_d(f)$ at the bandwidth

$$A(f) = Avg.\left(L_d(f)\right)_{f_1, f_2} \tag{7}$$

where the magnitudes of FFT corresponding to a frequency f_1 *to* f_2 at amplitude equal to $\frac{1}{\sqrt{2}}$ of peak amplitude in the FFT (**Figure 16b**).

Attenuation factor ($A(f)$) was calculated for all the received signals using Equation (7) and is shown in **Figure 17a**. There is no change in the attenuation factor even at very large crack openings for the transmission paths which do not encounter crack. There is a considerable decrease in the $A(f)$ for the transmission paths which encounters the crack, even at the stress-induced physical opening of 12 μm at the mid-height of the beam. The decrease in the attenuation factor values were high for signals received from PZTs placed at the soffit of the beam when compared with values of the signals received at the PZTs place at the mid-height of the beam. This is can be explained considering the crack opening in the direct stress wave path between an AR pair. The crack width opening along the depth of a specimen at different values of CMOD are shown in **Figure 10b**. The signals received at the PZTs placed at the soffit of the beam experienced a higher attenuation because of a larger physical opening in the direct path connecting the actuator to the receiver. Upon unloading, the physical discontinuity is larger in the stress wave path connecting PZT patches located on the beam soffit from actuators located across the crack. There is a complete attenuation of direct stress wave when the stress induced crack opening reaches a value of 100 μm.

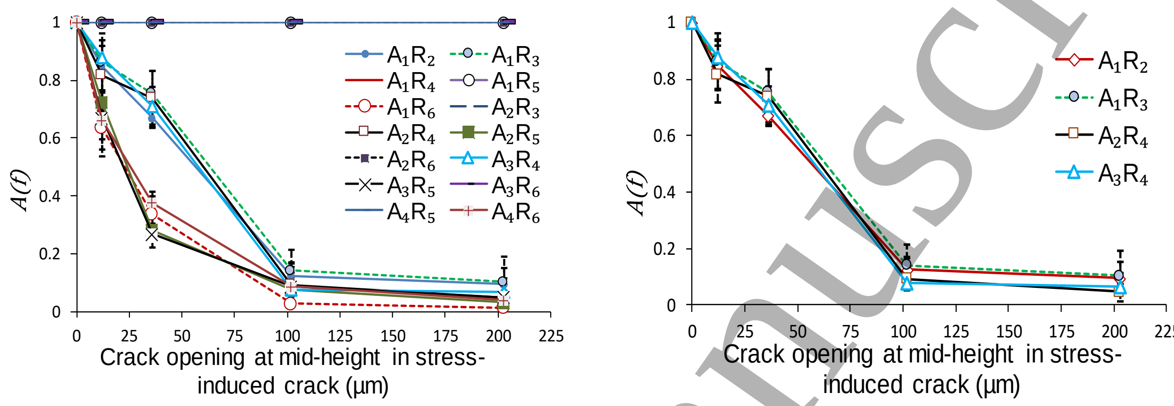

(a) (b)

Figure 17. Attenuation factor ($A(f)$) as a function of crack opening at mid-height in the stress induced crack (a) all AR pairs; (b) For AR pairs placed at the mid-height of the beam.

The changes in attenuation factor corresponding to the transmission paths which encounter a physical opening produced by a stress-induced crack and pass through center line of beam (actuator and receiver located in the mid-height of the beam) are shown in **Figure 17b.** For the PZTs mounted at the mid-height, the $A(f)$ is identical for the stress wave paths linking the AR pair which cross the crack plane. It can therefore be concluded that the observed $A(f)$ in these cases is only due to the magnitude of the physical discontinuity produced by the crack. The changes in $A(f)$ are only due to the changes in characteristics of discrete crack such as depth and width of crack, irrespective of length of signal transmission path. The similarity in the trends of changes in attenuation factor irrespective of length of signal transmission path also

644 suggests that the attenuation factor only depends on the severity of crack irrespective of all other intervening effects. The $A(f)$, therefore provides an effective way to analyze the received signals to detect changes introduced by material discontinuity in the stress wave path. The $A(f)$ is sensitive to a physical discontinuity in the concrete medium even in the unloaded state associated with a stress induced crack opening on the order of 10μm. The physical discontinuity in the concrete associated with a stress-induced crack opening on the order of 100 μm produces a complete attenuation of the stress wave. This indicates that there is no direct transmission of direct stress waves centered on 120 KHz across a physical discontinuity in concrete resulting from a stress-induced opening between the crack faces on the order of 0.1 mm.

A damage index derived from the RMSD is used to calculate the difference between the conductance signatures recorded for different crack openings. The RMSD with respect to the baseline measurement (zero CMOD) were calculated in the frequency range of the bandwidth for first and second resonant peaks using Equation (8), where, x_i and y_i are the values of baseline conductance and conductance at different CMOD levels and N is total number of frequencies in the bandwidth of the corresponding peak.

$$\text{RMSD} = \sqrt{\frac{\sum_{i=1}^{N}(y_i - x_i)^2}{\sum_{i=1}^{N}(x_i)^2}} \quad (8)$$

Damage index based on RMSD for PZTs of different positions are is shown in **Figure 18a**. The damage index was calculated using the frequency range of the bandwidth for second resonant peak. PZT3, which located 180 mm from the crack location registered a small change in the RMSD with increasing crack opening. PZT2 and PZT5, which are attached on the face and the soffit, respectively at the distances of 50 mm from the beam centerline show an increase in the RMSD with increasing CMOD. **Figure 18b** shows the RMSD calculated using first resonance peak in the frequency range of bandwidth. PZT3 is showing same RMSD trend as for second peak. There is a larger increase in value for RMSD at all CMOD values for PZT2 and PZT5 when comparing with RMSD of the second peak. The scatter in the RMSD values may be attributed to the irregular trend in the local peaks present on first resonance peak of the PZT.

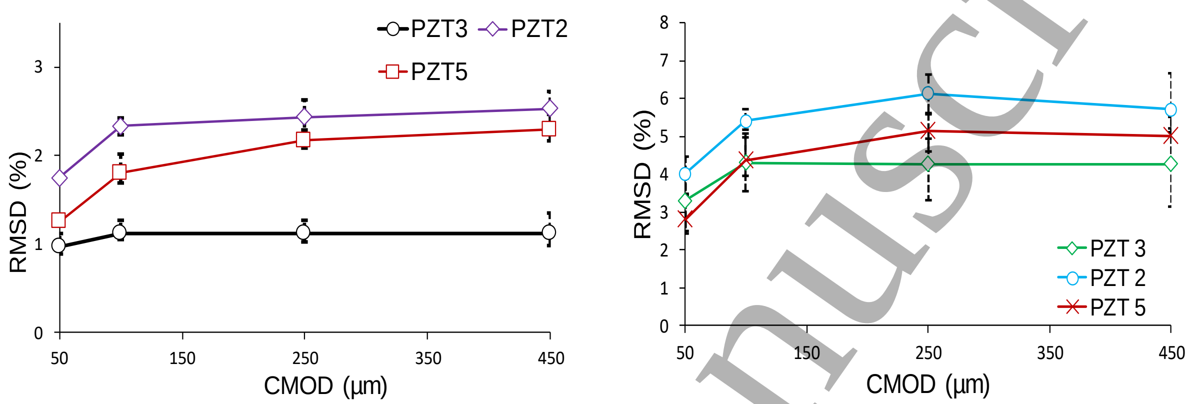

(a) (b)

Figure 18. RMSD (%) (a) Second resonance peak (b) First resonance peak

The measured RMSD detects changes in the first cycle while the changes in the subsequent load cycles are not significant. The RMSD measurements are indicative of changes in the material medium within the zone of influence produced by the discontinuity introduced by the crack. The discontinuity in the unloaded state represents the physical separation introduced in the material due to the stress-induced crack opening. The RMSD values indicate that the EI measurement is very sensitive in detecting the discontinuity more than the magnitude of the discontinuity. EI measurement would therefore provide a very sensitive measure of crack initiation in concrete in the vicinity of the PZT patch.

6. Summary and Findings

687 A combined local and distributed monitoring system for concrete structures using an array of surface mounted PZT patches is presented. EI impedance measurements from individual PZT patches are used for local monitoring while the through-transmission stress wave propagation technique is used for distributed sensing. Progression of discrete crack in concrete was evaluated using a full-field displacements measured on the surface of the beam obtained with the use digital image correlation and was correlated with measurements obtained from the PZT patches. The crack opening is mapped from a very small value on the order to 10 μm to 100 μm. The material away from the localized discontinuity produced by the crack is shown to relatively free from any damage.

696 Both the EI and the stress-wave propagation techniques are shown to be influenced by discontinuity in the concrete substrate produced by a stress-induced crack. The EI measurement is sensitive to the formation of localized damage in the form of a load induced crack in the vicinity of the PZT patch. A new damage index known as attenuation factor is introduced for the wave propagation technique. The attenuation factor is shown to be an effective damage index for detecting the severity of discontinuity produced by a crack. The attenuation factor is shown to determine attenuation of the wave produced by the discontinuity encountered by the direct stress wave, independent of the length of propagation. The attenuation measurements were performed in the unloaded state, where the removal of the load results in closing of the crack. The through transmission of direct stress wave through the medium is very sensitive to the presence of a discontinuity left in the medium resulting from a stress-induced crack in its path. There is an attenuation of the wave even for a physical discontinuity in the concrete in the stress free state associated with a small stress-induced crack opening on the order of 10 μm. There is a complete attenuation of the direct stress wave transmission at 120 kHz for physical discontinuity in the concrete associated with a stress-induced crack opening on the order of 100 μm.

The measurements from the PZT patches indicate that the localized discontinuity in concrete produced by a stress induced crack is easily detected using the attenuation factor from the direct stress wave transmission path. The stress-induced crack has considerable crack closing stresses provided by aggregates bridging the crack. The discontinuity in the unloaded state represents the physical separation introduced in the material due to the stress-induced crack opening. The cracks which would have propagated due to overloads, but are closed due to removal of the loads can therefore be easily be detected using attenuation factor measurements. This provides a very convenient measure for monitoring increment of damage due in the material. Further, crack opening on the order of 200 μm under service loads is often stipulated for durable design [ACI 224R-01 (2001), IS-456 (2000)]. The attenuation factor from distributed sensing provides for monitoring discontinuity in the material medium even in the unloaded state, when the crack is not visually detectable. The initiation of the discontinuity would be reflected in the EI signature if the discontinuity lies within its zone of influence. Service load condition of the concrete structure can therefore be monitored conveniently using combined EI and AR modes of an array of PZT patches.

References

[1] Achenbach, J.D., Komsky, I.N., Lee, Y.C. and Angel, Y.C., (1992), "Self-calibrating Ultrasonic Technique for Crack Depth Measurement," Journal of Nondestructive Evaluation, Vol.11, No.2, pp.103-108.

[2] ACI-224R-01., (2001), "Control of Cracking in Concrete Structures," Farmington Hills, MI: American Concrete Institute.

[3] Aggelis, D.G. and Shiotani, T., (2007), "Experimental Study of Surface Wave Propagation in Strongly Heterogeneous Media," The Journal of the Acoustical Society of America, Vol. 122, No. 5, pp.151-157.

[4] Bhalla S, and Soh CK (2004), "Structural Health Monitoring by Piezo-Impedance Transducers. I: Modeling," Journal of. Aerospace. Engineering, Vol. 17, No. 4, pp.154–165.

[5] Bruck, H.A., McNeill, S.R., Sutton, M.A, and Peters, W.H., (1989), "Digital Image Correlation Using the Newton Raphson Method of Partial Differential Correction," Experimental Mechanics, Vol. 29, No. 3, pp. 261-267.

[6] Divsholi, B.S. and Yang, Y., (2014), "Combined Embedded and Surface-bonded Piezoelectric Transducers for Monitoring of Concrete Structures," NDT & E International, Vol. 65, pp.28-34.

[7] Gali, S. and Subramaniam, K.V., (2018), "Multi-linear Stress-Crack Separation Relationship for Steel Fiber Reinforced Concrete: Analytical Framework and Experimental Evaluation," Theoretical and Applied Fracture Mechanics, Vol. 93, pp.33-43.

[8] Giurgiutiu, V. and Rogers, C.A., (1999), "Modeling of the Electro-mechanical (E/M) Impedance Response of a Damaged Composite Beam,". Adaptive Structures and Material Systems- November 14-19, pp.39-46.

[9] Giurgiutiu, V., (2001), "Structural Health Monitoring with Piezoelectric Active Sensors," Academic Press, Oxford, UK.

[10] Huo, L., Chen, D., Liang, Y., Li, H., Feng, X. and Song, G., (2017), "Impedance Based Bolt Pre-Load Monitoring Using Piezoceramic Smart Washer," Smart Materials and Structures, Vol. 26, No.5, p.057004.

[11] I.S 456: 2000, "Indian Standard-Plain and Reinforced Concrete Code of Practice".

759 [12] Jung, Y.C., Kundu, T. and Ehsani, M.R., (2002), "A New Nondestructive Inspection Technique for Reinforced Concrete Beams," ACI Materials Journal, Vol. 99, No. 3, pp.292-299.

762 [13] Kee, S.H. and Nam, B., (2015), "Automated Surface Wave Measurements for Evaluating the Depth of Surface-Breaking Cracks in Concrete," International Journal of Concrete Structures and Materials, Vol. 9, No. 3, pp.307-321.

765 [14] Liang, C., Sun, F.P., and Rogers, C.A., (1994), "An Impedance Method for Dynamic Analysis of Active Material Systems," Journal of Vibration and Acoustics, Vol.116, No.1, pp. 120-128.

768 [15] Liang, Y., Li, D., Parvasi, S.M., Kong, Q. and Song, G., (2016), "Bond-slip detection of concrete-encased composite structure using electro-mechanical impedance technique," Smart Materials and Structures, Vol.25, No.9, p.095003.

771 [16] Lim, Y Y., and Soh, C K., (2012), "Effect of varying axial load under fixed boundary condition on admittance signatures of electromechanical impedance technique," Journal of Intelligent Material Systems and Structures, doi: 10.1177/1045389X12437888.

774 [17] Lu, Y., Li, J., Ye, L. and Wang, D., (2013), "Guided Waves for Damage Detection in Rebar-reinforced Concrete Beams," Construction and Building Materials, Vol. 47, pp.370-378.

777 [18] Luo, M., Li, W., Hei, C. and Song, G., (2016), "Concrete Infill Monitoring in Concrete-Filled FRP Tubes Using a PZT-Based Ultrasonic Time-of-Flight Method," Sensors, Vol. 16, No. 12, p.2083.

780 [19] Memmolo, V., Maio, L., Boffa, N.D., Monaco, E. and Ricci, F., (2016), "Damage Detection Tomography Based on Guided Waves in Composite Structures Using a Distributed Sensor Network," Optical Engineering, Vol. 55, No.1, pp.011007-011007.

[20] Moradi-Marani, F., Rivard, P., Lamarche, C.P. and Kodjo, S.A., (2014), "Evaluating the Damage in Reinforced Concrete Slabs Under Bending Test with the Energy of Ultrasonic Waves," Construction and Building Materials, Vol. 73, pp.663-673.

[21] Na, S. and Lee, H.K., (2012), "A technique for improving the damage detection ability of the electro-mechanical impedance method on concrete structures," Smart Materials and Structures, Vol.21, No.8, p.085024.

[22] Narayanan, A., and Subramaniam, K V L., (2016a), "Experimental evaluation of load-induced damage in concrete from distributed microcracks to localized cracking on electro-mechanical impedance response of bonded PZT", Construction and Building Materials, Vol.105, pp. 536-544.

[23] Narayanan, A., and Subramaniam, K. V. L., (2016b), "Sensing of Damage and Substrate Stress in Concrete Using Electro-Mechanical Impedance Measurements of Bonded PZT Patches", Smart Materials and Structures, Vol. 25, No. 9, p.095011.

[24] Narayanan, A., Kocherla, A. and Subramaniam, K.V., (2017), "Embedded PZT Sensor for Monitoring Mechanical Impedance of Hydrating Cementitious Materials," Journal of Nondestructive Evaluation, Vol. 36, No. 4, p.64.

[25] Narayanan, A., Kocherla, A. and Subramaniam, K.V.L., (2018), "Understanding the Coupled Electromechanical response of PZT attached to Concrete: Influence of Substrate size," under review in Measurement.

[26] Park, G., Cudney, H., and Inman, D., (2000), "Impedance-Based Health Monitoring of Civil Structural Components," Journal of Infrastructure Systems, Vol.6, No.4, pp. 153–160.

[27] Park, S., Ahmad, S., Yun, C.B. and Roh, Y., (2006), "Multiple Crack Detection of Concrete Structures Using Impedance-based Structural Health Monitoring Techniques," Experimental Mechanics, Vol. 46, No.5, pp.609-618.

[28] Reddy, K.C. and Subramaniam, K.V., (2017), "Analysis for multi-linear stress-crack opening cohesive relationship: Application to macro-synthetic fiber reinforced concrete," Engineering Fracture Mechanics, Vol. 169, pp.128-145.

[29] Rucka, M. and Wilde, K., (2013), "Experimental Study on Ultrasonic Monitoring of Splitting Failure in Reinforced Concrete," Journal of Nondestructive evaluation, Vol. 32, No. 4, pp.372-383.

[30] Schreier, H, and Sutton, M., (2002), "Systematic Errors in Digital Image Correlation Due to Undermatched Subset Shape functions," Experimental Mechanics, Vol.42, No.3, pp. 303-310.

[31] Song, F., Huang, G.L., Kim, J.H. and Haran, S., (2008), "On the Study of Surface Wave Propagation in Concrete Structures Using a Piezoelectric Actuator/Sensor System,". Smart Materials and Structures, Vol. 17, No. 5, p.055024.

[32] UNI 11039-2: 2003, "Steel Fibre Reinforced Concrete - Test Method for Determination of First Crack Strength and Ductility Indexes. National Italian Unification Centre,", Italy.

[33] Wang, X. and Subramaniam, K.V., (2011), "Ultrasonic Monitoring of Capillary Porosity and Elastic Properties in Hydrating Cement Paste," Cement and Concrete Composites, Vol.33, No.3, pp.389-401.

[34] Watanabe, T., Trang, H.T.H., Harada, K. and Hashimoto, C., (2014), "Evaluation of Corrosion-Induced Crack and Rebar Corrosion by Ultrasonic Testing," Construction and Building Materials, Vol.67, pp.197-201.

[35] Xu, B., Chen, H. and Xia, S., (2017), "Numerical Study on The Mechanism of Active Interfacial Debonding Detection for Rectangular CFSTs Based on Wavelet Packet Analysis with Piezoceramics," Mechanical Systems and Signal Processing, Vol. 86, pp.108-121.

[36] Xu, Y.G., and Liu, G.R., (2002), "A Modified Electro-Mechanical Impedance Model of Piezoelectric Actuator-Sensors for Debonding Detection of Composite Patches," Journal of Intelligent Material Systems and Structures, Vol. 13, No. 6, pp. 389-396.

[37] Zagrai, A.N. and Giurgiutiu, V., (2001), "Electro-Mechanical Impedance Method for Crack Detection in Thin Plates," Journal of Intelligent Material Systems and Structures, Vol. 12, No. 10, pp.709-718.

[38] Zhu, J. and He, L., (2011), "Study on Piezoelectric Wave Propagation Based Nondestructive Monitoring Method of Concrete," In IEEE International Conference on Electric Technology and Civil Engineering (ICETCE), pp. 764-767.